JACS
JOURNAL OF THE AMERICAN CHEMICAL SOCIETY

Communication

pubs.acs.org/JACS

A Redox-Active Bistable Molecular Switch Mounted inside a Metal–Organic Framework

Qishui Chen,[†,§] Junling Sun,[†,§] Peng Li,[†] Idan Hod,[†] Peyman Z. Moghadam,[‡,⊥] Zachary S. Kean,[†] Randall Q. Snurr,[‡] Joseph T. Hupp,*[,†] Omar K. Farha,*[,†,∥] and J. Fraser Stoddart*[,†]

Departments of [†]Chemistry and [‡]Chemical and Biological Engineering, Northwestern University, Evanston, Illinois 60208, United States

[∥]Department of Chemistry, Faculty of Science, King Abdulaziz University, Jeddah 21589, Saudi Arabia

Supporting Information

ABSTRACT: We describe the incorporation of a bistable mechanically interlocked molecule (MIM) into a robust Zr-based metal–organic framework (MOF), **NU-1000**, by employing a post-synthetic functionalization protocol. On average, close to two bistable [2]catenanes can be incorporated per repeating unit of the hexagonal channels of **NU-1000**. The reversible redox-switching of the bistable [2]catenanes is retained inside the MOF, as evidenced by solid-state UV-vis-NIR reflectance spectroscopy and cyclic voltammetry. This research demonstrates that bistable MIMs are capable of exhibiting robust dynamics inside the nanopores of a MOF.

The emergence of mechanically interlocked molecules[1] (MIMs) during the past few decades has progressed from degenerate molecular shuttles[2] to artificial molecular switches[3] (AMSs) and machines[4] (AMMs). Bistable MIMs[5,6] have been designed and synthesized with component parts that can be induced to move mechanically with respect to each other under the influence of external stimuli, resulting in the operation of two-state (on/off) switches that have found application in molecular electronic devices[7] (MEDs) and drug delivery systems.[8] By contrast with AMSs and AMMs devoid[9] of mechanical bonds, bistable MIMs[5,6] involve induced relative mechanical motions of component parts within molecules—for example, the circumrotation of one ring with respect to another in a bistable [2]catenane[5] and the translation of a ring along a dumbbell in a bistable [2]rotaxane.[6] Switching between the two states in these bistable MIMs[5,6] can be controlled by light[10] or by changes in pH[11] or redox properties.[12] The modulation of weak noncovalent bonding interactions such as hydrogen-bonding,[11] donor-acceptor,[12] and radical-pairing[13] in the two states allows us to alter the chemical and physical properties of bistable MIMs. These mechanically activated molecules, however, are plagued by incoherence because of their random motions in solution. Consequently, they have been located at interfaces as Langmuir–Blodgett films[14] as well as in the form of self-assembled monolayers on flat gold surfaces[15] and on metal nanoparticles.[16] A challenge of introducing bistable MIMs into MEDs[7] is to create a rigid scaffolding in which their solution-state switching is maintained, but occurs in unison, and their on/off states can be interrogated in a collective manner.

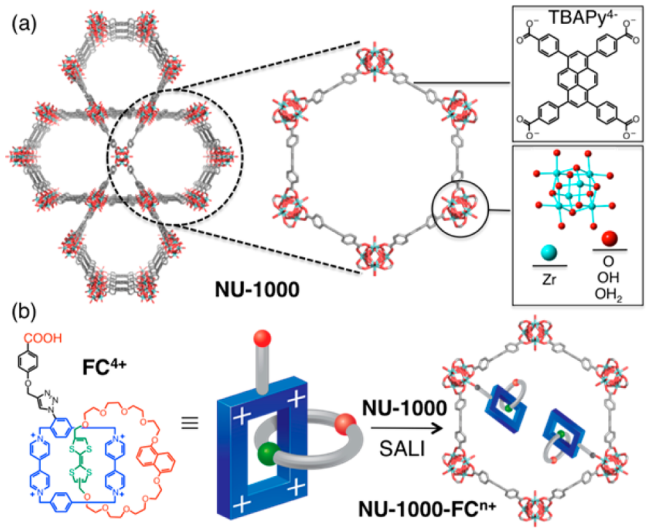

Figure 1. (a) Structure of **NU-1000** (red, oxygen; blue, zirconium; gray, carbon). (b) Schematic of the functionalized bistable [2]catenane FC^{4+} organized into **NU-1000** by the SALI approach.

The concept of robust dynamics[17] envisages the mounting of bistable MIMs inside metal–organic frameworks (MOFs) as a means of enhancing significantly the order, coherence, and performance of the MIMs while, at the same time, protecting their component parts from degradation during the switching process. While our attempts to incorporate crown ethers,[18] capable of binding substrates, and [2]catenanes,[19] proficient in displaying ring circumrotations, into the struts of MOFs have met with only limited success, Loeb[20] has shown that large-amplitude motions by rings encircling struts can undergo degenerate switching and rotation within the lattices of MOFs at high temperatures.

Recently, we reported[21] the organized insertion of electrochemically addressable tricationic trisradical rotaxanes within the channels of a Zr-based MOF (**NU-1000**) post-synthetically using a solvent-assisted ligand incorporation (SALI) protocol.[22] In this Communication, we describe the incorporation (Figure 1) of a functionalized bistable redox-switchable [2]catenane, FC^{4+}, into **NU-1000** using the SALI protocol. The donor-

Received: September 20, 2016
Published: October 24, 2016

DOI: 10.1021/jacs.6b09880
J. Am. Chem. Soc. 2016, 138, 14242–14245

acceptor [2]catenane[5] is comprised of a tetracationic cyclophane, cyclo(bisparaquat-*p*-phenylene) (CBPQT^{4+}), mechanically interlocked by a macrocyclic polyether containing electron-rich tetrathiafulvalene (TTF) and 1,5-dioxynaphthalene (DNP) recognition sites.[7] We report (i) qualitative evidence, with quantitative backing, for the incorporation of a suitably functionalized [2]catenane **FC**$^{4+}$ into **NU-1000**, along with (ii) adsorption isotherms and calculated pore size distributions, (iii) cyclic voltammetry (CV) performed on **FC**$^{4+}$ in solution and **NU-1000-FC**$^{n+}$ embedded in thin films, and (iv) chemical redox of **NU-1000-FC**$^{n+}$ monitored by solid-state UV-vis-NIR reflectance spectroscopy, showing that **FC**$^{4+}$ can be switched reversibly inside **NU-1000**.

Figure 1 outlines the strategy for attaching **FC**$^{4+}$ inside **NU-1000**, which consists of octahedral Zr_6 nodes with bridging 1,3,6,8-tetrakis(*p*-benzoic acid)pyrene (H_4TBAPy) linkers.[23] Each metal cluster is capped by eight bridging hydroxyl and oxo ligands, while the remaining coordination sites are occupied by terminal OH and OH_2 ligands. They provide a platform for SALI-style post-synthetic modification between carboxylic acid functions and the terminal hydroxyl groups that point into the wide mesoporous channels. At the outset, we functionalized the bistable [2]catenane with a benzoic acid linker using Cu(I)-catalyzed azide-alkyne cycloaddition to prepare the precursor, **FC**$^{4+}$, for SALI. The carboxylic acid functionality was introduced by reacting 4-(propargyloxy)benzoic acid with an azide-functionalized CBPQT^{4+} derivative.[24] This acid-functionalized CBPQT^{4+} precursor, when reacted with the appropriate macrocyclic polyether in a thermodynamically controlled reaction[25] in the presence of tetrabutylammonium iodide, afforded the bistable [2]catenane **FC**$^{4+}$ (see Supporting Information (SI)). Compared with the analogous rotaxane featuring the same recognition sites, the bistable catenane molecules are much more compact, making them ideal for SALI. They can also be assembled prior to SALI to ensure that all the incorporated molecules are mechanically interlocked.

SALI was carried out by heating a microcrystalline yellow powder of activated **NU-1000** in an MeCN solution of **FC**$^{4+}$ at 60 °C for 48 h to afford **NU-1000-FC**$^{n+}$ as a green powder (see SI). The degree of incorporation was characterized by ^{1}H NMR spectroscopy of the digested **NU-1000-FC**$^{n+}$ (SI, Figure S4). The proton resonances of the [2]catenane were integrated against the TBAPy ligand, showing that ~0.46−0.67 equiv of **FC**$^{4+}$ is incorporated onto each Zr_6 node within **NU-1000**. We employed inductively coupled plasma−atomic emission spectroscopy (ICP-AES) to obtain a more accurate degree of functionalization, where the loading of **FC**$^{4+}$ was determined by comparing the S:Zr ratio in the sample. Elemental analysis revealed the incorporation of 0.65 equiv of **FC**$^{4+}$ per node. Finally, we used scanning electron microscopy−energy dispersive X-ray spectroscopy (SEM-EDX) to investigate (SI, Figure S8) the distribution of **FC**$^{4+}$ within individual **NU-1000** microcrystals. Both Zr and S were detected throughout the entire crystal, and their distribution was found to be homogeneous.

The density functional theory (DFT) pore size distributions and N_2 adsorption isotherms for **NU-1000** and **NU-1000-FC**$^{n+}$ are shown in Figure 2. The N_2 adsorption isotherms retain the type IV shape of the parent **NU-1000**. Brunauer−Emmett−Teller analyses indicate a decrease in surface area from 2200 to 2020 m^2/g following SALI. The DFT pore size distributions, extracted from the isotherms, indicate that the second peak, corresponding to the mesopore—namely, the hexagonal one—

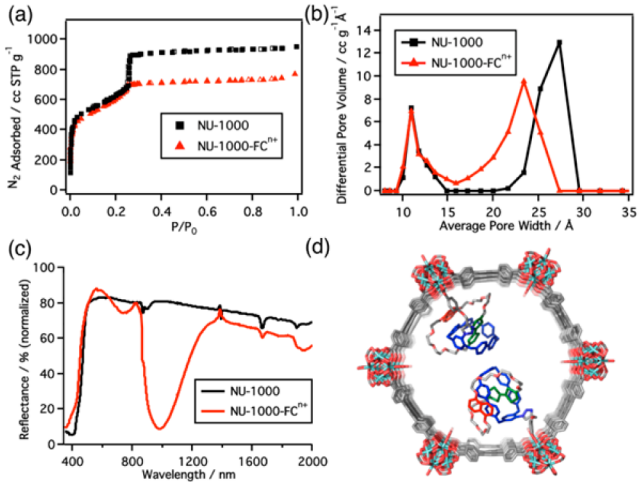

Figure 2. (a) N_2 adsorption isotherms and (b) DFT pore size distributions for **NU-1000** and **NU-1000-FC**$^{n+}$. (c) Solid-state UV-vis-NIR reflectance of **NU-1000** and **NU-1000-FC**$^{n+}$. (d) Molecular mechanics model of the spatial distribution of **FC**$^{4+}$ within the hexagonal pore of **NU-1000**.

shows a decrease in pore diameter from 28 to 23 Å, as well as in differential pore volume from 13 to 10 cm^3/(g·Å). Meanwhile, the pore volume and size for the triangular channel remain the same. These data suggest that **FC**$^{4+}$ is located primarily in the hexagonal channels. Combined with the information relating to the degree of functionalization, it gives, on average, nearly two bistable [2]catenanes functionalized per hexagonal pore.

The successful formation of **NU-1000-FC**$^{n+}$ has been confirmed by solid-state UV-vis-NIR reflectance measurements. The parent **NU-1000** shows (Figure 2c) a reflectance peak centered around 400 nm, arising from the pyrene ligands. Following SALI, a new peak emerges, spanning 800−1200 nm, indicative of charge transfer between CBPQT^{4+} and TTF. This observation is consistent with solution studies carried out (SI, Figure S6) on **FC**$^{4+}$, where the CBPQT^{4+} ring encircles the TTF recognition unit. Molecular mechanics modeling of a short section of the hexagonal pore containing two bistable [2]catenanes indicates (Figure 2d) that there is sufficient free volume for the components to pack without significant distortions. Comparison of the energies of **NU-1000-FC**$^{n+}$ versus the isolated analogues also indicates that there is only a small increase in the destabilization due to steric interactions on going from incorporation of one catenane (+56 kcal/mol) to two catenanes (+84 kcal/mol). Although the effects of solvents and counterions are not taken into account in the model, the difference in energies supports the experimental observation of incorporating up to two bistable [2]catenanes per hexagonal pore. See SI for computational details.

The redox properties of **FC**$^{4+}$ in solution were investigated (Figure 3a, top) by CV. In the positive region, the voltammogram displays one 2e$^-$ oxidation at +878 mV, which represents both the 1e$^-$ oxidation of the encircled TTF unit (TTF→TTF$^{(\bullet+)}$) and the 1e$^-$ oxidation of the free TTF$^{(\bullet+)}$→TTF^{2+}. The initial TTF oxidation is shifted to a more anodic potential as a result of the stabilization of the CBPQT^{4+} ring surrounding the TTF unit.[26] Upon oxidation to the radical cationic TTF$^{(\bullet+)}$, CBPQT^{4+} encircles the DNP unit as a result of Coulombic repulsions. The negative region of the voltammogram displays reversible reduction peaks of the pyridinium units in CBPQT^{4+}. These findings are consistent

DOI: 10.1021/jacs.6b09880
J. Am. Chem. Soc. 2016, 138, 14242−14245

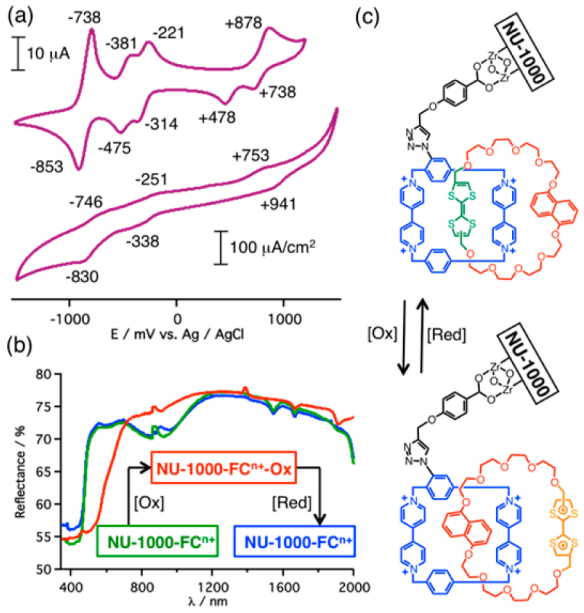

Figure 3. (a) Cyclic voltammograms of $\mathbf{FC}^{4+}$ (1 mM in MeCN, 0.1 M $TBAPF_6$, 200 mV/s, top) and thin film of **NU-1000-FC**$^{n+}$ on FTO (0.1 M $TBAPF_6$ in MeCN, 200 mV/s, bottom). (b) Reversible switching of **NU-1000-FC**$^{n+}$ by chemical oxidation/reduction. UV-vis-NIR spectra show the disappearance (red) and subsequent re-emergence (blue) of the characteristic charge-transfer band between TTF and $CBPQT^{4+}$. (c) Schematic of the reversible switching of **NU-1000-FC**$^{n+}$.

with previous reports on TTF- and $CBPQT^{4+}$-containing catenanes.[5,26]

It is well known that, in redox-active MOF-based thin films, electrochemical charge transport is achieved by a relatively slow, diffusive redox hopping mechanism, following an energetically symmetric electron self-exchange from one redox-active unit to another.[27] Thus, when measuring the electrochemical activity of **NU-1000-FC**$^{n+}$ thin films (Figure 3a, bottom), we were able to detect two reversible peaks at −338 and −830 mV, corresponding to the reduction of the bipyridinium units, consistent with solution studies of $\mathbf{FC}^{4+}$. When the potential was scanned in the positive direction, an oxidation peak for TTF appeared around +753 mV. Notably, a broad TTF reduction peak appeared at a more anodic (positive) potential compared to its corresponding oxidation potential. To understand this behavior, we ran additional control CV experiments, in which we scanned (SI, Figure S5) to different anodic potentials to monitor the contribution of pyrene oxidation to the system's electrochemical response.[28] At more anodic scans, a large oxidation peak appears, corresponding to the pyrene-based linker oxidation. In addition, the intensity of the TTF reduction peak diminishes dramatically when scanning to lower potentials, where no pyrene oxidation is detected. This behavior could possibly be attributed to the pyrene radical cation reduction, mediated by the redox-active TTF unit attached to the MOF node.[29] Similar effects were observed previously[28b] with **NU-1000** tethered with a ferrocene redox shuttle, mediating the redox activity of Fe and Co bipyridine couples in solution.

To examine whether the circumrotational motion of the macrocyclic polyether in $\mathbf{FC}^{4+}$ is retained in the solid state, we analyzed the switching behavior of **NU-1000-FC**$^{n+}$ by a chemical oxidation/reduction cycle. The choice of oxidizing and reducing agents, 2,3-dichloro-5,6-dicyano-1,4-benzoquinone (DDQ) and ascorbic acid, respectively, is based on the potential window from electrochemical studies, where they are only active toward the TTF unit as opposed to the TBAPy ligands in **NU-1000** or the $CBPQT^{4+}$ ring. This selection ensures that the MOF behaves as an inert substrate and its structure remains intact throughout the switching process (SI, Figure S9). The UV-vis-NIR spectra of powder samples of **NU-1000-FC**$^{n+}$ (green) upon oxidation (red) and subsequent reduction (blue) are shown in Figure 3b. Upon oxidation with DDQ, the characteristic TTF⊂$CBPQT^{4+}$ charge-transfer band around 800−1200 nm disappears, indicating that the macrocyclic polyether has undergone circumrotation such that the DNP unit resides within the $CBPQT^{4+}$ ring. Treatment of the oxidized sample with ascorbic acid recovers the original spectrum, demonstrating that $\mathbf{FC}^{4+}$ can be switched reversibly inside **NU-1000**, thus achieving dynamic behavior within an ordered, robust material. Previous examples of dynamic systems in MOFs have featured molecular rotors[24b] and shuttles,[20b] where the motion of the individual components cannot be controlled. By utilizing a bistable MIM with redox-active recognition sites, we have demonstrated a system where the motion of the macrocyclic polyether between two recognition sites can be switched reversibly and predictably inside a highly organized framework.

This investigation describes the implantation of a bistable molecular switch within a crystalline MOF. The post-synthetic modification employed to attach the bistable [2]catenane molecules inside **NU-1000** not only eliminates the need for multiple-step syntheses of organic struts containing bistable MIMs but also positions them inside the mesoporous channels which provide the free volume that is essential for them to retain their switching dynamics. On average, nearly two bistable catenanes can be incorporated into each hexagonal pore of **NU-1000**, achieving a highly organized and densely packed material of up to 8.8×10^{19} units/cm^3. Moreover, the redox-switching properties of the bistable catenane are retained in the solid-state material. We believe this technological advance represents an important step toward incorporating bistable MIMs into robust, highly porous frameworks as prototypes for molecular electronic devices.

■ ASSOCIATED CONTENT

Supporting Information

The Supporting Information is available free of charge on the ACS Publications website at DOI: 10.1021/jacs.6b09880.

Synthetic procedures, ^{1}H and ^{13}C NMR, CV, UV-vis-NIR, SEM-EDX, PXRD, and molecular mechanics modeling (PDF)

■ AUTHOR INFORMATION

Corresponding Authors

*j-hupp@northwestern.edu
*o-farha@northwestern.edu
*stoddart@northwestern.edu

Present Address

⊥P.Z.M.: Department of Chemical Engineering & Biotechnology, University of Cambridge, Cambridge, U.K.

Author Contributions

§Q.C. and J.S. contributed equally to this work.

DOI: 10.1021/jacs.6b09880
J. Am. Chem. Soc. 2016, 138, 14242−14245

Notes

The authors declare no competing financial interest.

■ ACKNOWLEDGMENTS

This research is part of the Joint Center of Excellence in Integrated Nano-Systems (JCIN) at King Abdulaziz City for Science and Technology (KACST) and Northwestern University (NU). The authors thank KACST and NU for their continued support of this research and gratefully acknowledge support from the International Institute for Nanotechnology at NU (Z.S.K.), U.S. DOE, Office of Science, Basic Energy Sciences (grant no. DE-FG02-87ER13808, J.T.H.), and NU (O.K.F.).

■ REFERENCES

(1) (a) Dietrich-Buchecker, C. O.; Sauvage, J.-P. *Chem. Rev.* **1987**, *87*, 795. (b) Amabilino, D. B.; Stoddart, J. F. *Chem. Rev.* **1995**, *95*, 2725. (c) Stoddart, J. F. *Chem. Soc. Rev.* **2009**, *38*, 1802. (d) van Dongen, S. F.; Cantekin, S.; Elemans, J. A. A. W.; Rowan, A. E.; Nolte, R. J. M. *Chem. Soc. Rev.* **2014**, *43*, 99. (e) Gil-Ramírez, G.; Leigh, D. A.; Stephens, A. J. *Angew. Chem., Int. Ed.* **2015**, *54*, 6110.

(2) (a) Anelli, P.-L.; Spencer, N.; Stoddart, J. F. *J. Am. Chem. Soc.* **1991**, *113*, 5131. (b) Loeb, S. J.; Wisner, J. A. *Chem. Commun.* **2000**, 1939. (c) Günbas, D. D.; Brouwer, A. M. *J. Org. Chem.* **2012**, *77*, 5724.

(3) (a) Bissell, R. A.; Córdova, E.; Kaifer, A. E.; Stoddart, J. F. *Nature* **1994**, *369*, 133. (b) Livoreil, A.; Dietrich-Buchecker, C. O.; Sauvage, J.-P. *J. Am. Chem. Soc.* **1994**, *116*, 9399. (c) Sun, J.; Wu, Y.; Wang, Y.; Liu, Z.; Cheng, C.; Hartlieb, K. J.; Wasielewski, M. R.; Stoddart, J. F. *J. Am. Chem. Soc.* **2015**, *137*, 13484.

(4) (a) Sauvage, J.-P. *Acc. Chem. Res.* **1998**, *31*, 611. (b) Coskun, A.; Banaszak, M.; Astumian, R. D.; Stoddart, J. F.; Grzybowski, B. A. *Chem. Soc. Rev.* **2012**, *41*, 19. (c) Kay, E. R.; Leigh, D. A. *Angew. Chem., Int. Ed.* **2015**, *54*, 10080. (d) Erbas-Cakmak, S.; Leigh, D. A.; McTernan, C. T.; Nussbaumer, A. L. *Chem. Rev.* **2015**, *115*, 10081. (e) Peplow, M. *Nature* **2015**, *525*, 18.

(5) Asakawa, M.; Ashton, P. R.; Balzani, V.; Credi, A.; Hamers, C.; Mattersteig, G.; Montalti, M.; Shipway, A. N.; Spencer, N.; Stoddart, J. F.; Tolley, M. S.; Venturi, M.; White, A. J. P.; Williams, D. J. *Angew. Chem., Int. Ed.* **1998**, *37*, 333.

(6) Tseng, H.-R.; Vignon, S. A.; Stoddart, J. F. *Angew. Chem., Int. Ed.* **2003**, *42*, 1491.

(7) (a) Collier, C. P.; Mattersteig, G.; Wong, E. W.; Luo, Y.; Beverly, K.; Sampaio, J.; Raymo, F. M.; Stoddart, J. F.; Heath, J. R. *Science* **2000**, *289*, 1172. (b) Green, J. E.; Choi, J. W.; Boukai, A.; Bunimovich, Y.; Johnston-Halperin, E.; DeIonno, E.; Luo, Y.; Sheriff, B. A.; Xu, K.; Shin, Y. S.; Tseng, H. R.; Stoddart, J. F.; Heath, J. R. *Nature* **2007**, *445*, 414. (c) Coskun, A.; Spruell, J. M.; Barin, G.; Dichtel, W. R.; Flood, A. H.; Botros, Y. Y.; Stoddart, J. F. *Chem. Soc. Rev.* **2012**, *41*, 4827.

(8) Li, Z.; Barnes, J. C.; Bosoy, A.; Stoddart, J. F.; Zink, J. I. *Chem. Soc. Rev.* **2012**, *41*, 2590.

(9) (a) Feringa, B. L. *J. Org. Chem.* **2007**, *72*, 6635. (b) Michl, J.; Sykes, E. C. H. *ACS Nano* **2009**, *3*, 1042. (c) Vogelsberg, C. S.; Garcia-Garibay, M. A. *Chem. Soc. Rev.* **2012**, *41*, 1892. (d) Tatum, L. A.; Su, X.; Aprahamian, I. *Acc. Chem. Res.* **2014**, *47*, 2141.

(10) (a) Berna, J.; Leigh, D. A.; Lubomska, M.; Mendoza, S. M.; Perez, E. M.; Rudolf, P.; Teobaldi, G.; Zerbetto, F. *Nat. Mater.* **2005**, *4*, 704. (b) Balzani, V.; Clemente-Leon, M.; Credi, A.; Ferrer, B.; Venturi, M.; Flood, A. H.; Stoddart, J. F. *Proc. Natl. Acad. Sci. U.S.A.* **2006**, *103*, 1178. (c) Ragazzon, G.; Baroncini, M.; Silvi, S.; Venturi, M.; Credi, A. *Nat. Nanotechnol.* **2015**, *10*, 70.

(11) (a) Blanco, V.; Carlone, A.; Hanni, K. D.; Leigh, D. A.; Lewandowski, B. *Angew. Chem., Int. Ed.* **2012**, *51*, 5166. (b) Grunder, S.; McGrier, P. L.; Whalley, A. C.; Boyle, M. M.; Stern, C.; Stoddart, J. F. *J. Am. Chem. Soc.* **2013**, *135*, 17691.

(12) Fahrenbach, A. C.; Bruns, C. J.; Li, H.; Trabolsi, A.; Coskun, A.; Stoddart, J. F. *Acc. Chem. Res.* **2014**, *47*, 482.

(13) Trabolsi, A.; Khashab, N.; Fahrenbach, A. C.; Friedman, D. C.; Colvin, M. T.; Cotí, K. K.; Benítez, D.; Tkatchouk, E.; Olsen, J.-C.; Belowich, M. E.; Carmielli, R.; Khatib, H. A.; Goddard, W. A., III; Wasielewski, M. R.; Stoddart, J. F. *Nat. Chem.* **2010**, *2*, 42.

(14) Norgaard, K.; Laursen, B. W.; Nygaard, S.; Kjaer, K.; Tseng, H. R.; Flood, A. H.; Stoddart, J. F.; Bjornholm, T. *Angew. Chem., Int. Ed.* **2005**, *44*, 7035.

(15) Tseng, H.-R.; Wu, D.; Fang, N. X.; Zhang, X.; Stoddart, J. F. *ChemPhysChem* **2004**, *5*, 111.

(16) Coskun, A.; Wesson, P. J.; Klajn, R.; Trabolsi, A.; Fang, L.; Olson, M. A.; Dey, S. K.; Grzybowski, B. A.; Stoddart, J. F. *J. Am. Chem. Soc.* **2010**, *132*, 4310.

(17) Deng, H.; Olson, M. A.; Stoddart, J. F.; Yaghi, O. M. *Nat. Chem.* **2010**, *2*, 439.

(18) (a) Li, Q.; Zhang, W.; Miljanić, O. Š.; Sue, C.-H.; Zhao, Y.-L.; Liu, L.; Knobler, C. B.; Stoddart, J. F.; Yaghi, O. M. *Science* **2009**, *325*, 855. (b) Zhao, Y.-L.; Liu, L.; Zhang, W.; Sue, C.-H.; Li, Q.; Miljanić, O. Š.; Yaghi, O. M.; Stoddart, J. F. *Chem.-Eur. J.* **2009**, *15*, 13356.

(19) (a) Li, Q.; Zhang, W.; Miljanić, O. Š.; Knobler, C. B.; Stoddart, J. F.; Yaghi, O. M. *Chem. Commun.* **2010**, *46*, 380. (b) Sue, A. C.-H.; Mannige, R. V.; Deng, H.; Cao, D.; Wang, C.; Gándara, F.; Stoddart, J. F.; Whitelam, S.; Yaghi, O. M. *Proc. Natl. Acad. Sci. U.S.A.* **2015**, *112*, 5591.

(20) (a) Vukotic, V. N.; Harris, K. J.; Zhu, K.; Schurko, R. W.; Loeb, S. J. *Nat. Chem.* **2012**, *4*, 456. (b) Zhu, K.; O'Keefe, C. A.; Vukotic, V. N.; Schurko, R. W.; Loeb, S. J. *Nat. Chem.* **2015**, *7*, 514.

(21) McGonigal, P. R.; Deria, P.; Hod, I.; Moghadam, P. Z.; Avestro, A.-J.; Horwitz, N. E.; Gibbs-Hall, I. C.; Blackburn, A. K.; Chen, D.; Botros, Y. Y.; Wasielewski, M. R.; Snurr, R. Q.; Hupp, J. T.; Farha, O. K.; Stoddart, J. F. *Proc. Natl. Acad. Sci. U.S.A.* **2015**, *112*, 11161.

(22) (a) Deria, P.; Mondloch, J. E.; Tylianakis, E.; Ghosh, P.; Bury, W.; Snurr, R. Q.; Hupp, J. T.; Farha, O. K. *J. Am. Chem. Soc.* **2013**, *135*, 16801. (b) Deria, P.; Mondloch, J. E.; Karagiaridi, O.; Bury, W.; Hupp, J. T.; Farha, O. K. *Chem. Soc. Rev.* **2014**, *43*, 5896.

(23) Wang, T. C.; Vermeulen, N. A.; Kim, I. S.; Martinson, A. B.; Stoddart, J. F.; Hupp, J. T.; Farha, O. K. *Nat. Protoc.* **2016**, *11*, 149.

(24) The propargyloxy spacer was chosen to create a distance of sufficient magnitude between the tethered $\mathbf{FC}^{4+}$ catenanes and the TBAPy struts, providing the free volume that is essential for maintaining switching of the bistable $\mathbf{FC}^{4+}$ catenane inside **NU-1000**. See: (a) Khuong, T. A. V.; Nunez, J. E.; Godinez, C. E.; Garcia-Garibay, M. A. *Acc. Chem. Res.* **2006**, *39*, 413. (b) Gould, S. L.; Tranchemontagne, D.; Yaghi, O. M.; Garcia-Garibay, M. A. *J. Am. Chem. Soc.* **2008**, *130*, 3246.

(25) Miljanić, O. Š.; Stoddart, J. F. *Proc. Natl. Acad. Sci. U.S.A.* **2007**, *104*, 12966.

(26) The oxidation of the TTF unit in $\mathbf{FC}^{4+}$ is shifted slightly to more anodic potential compared with that of the parent unfunctionalized catenane. (See: Fahrenbach, A. C.; Barnes, J. C.; Li, H.; Benítez, D.; Basuray, A. N.; Fang, L.; Sue, C.-H.; Barin, G.; Dey, S. K.; Goddard, W. A., III; Stoddart, J. F. *Proc. Natl. Acad. Sci. U.S.A.* **2011**, *108*, 20416 .) We attribute this observation to the presence of a higher circumrotational barrier in $\mathbf{FC}^{4+}$ brought about by the acid linker.

(27) (a) D'Alessandro, D. M. *Chem. Commun.* **2016**, *52*, 8957. (b) Ahrenholtz, S. R.; Epley, C. C.; Morris, A. J. *J. Am. Chem. Soc.* **2014**, *136*, 2464.

(28) Previous electrochemical studies on **NU-1000** indicate that the electro-oxidation of TBAPy occurs around 1.6 V vs Ag/AgCl in organic solvents. See: (a) Kung, C.-W.; Wang, T. C.; Mondloch, J. E.; Fairen-Jimenez, D.; Gardner, D. M.; Bury, W.; Klingsporn, J. M.; Barnes, J. C.; Van Duyne, R.; Stoddart, J. F.; Wasielewski, M. R.; Farha, O. K.; Hupp, J. T. *Chem. Mater.* **2013**, *25*, 5012. (b) Hod, I.; Bury, W.; Gardner, D. M.; Deria, P.; Roznyatovskiy, V.; Wasielewski, M. R.; Farha, O. K.; Hupp, J. T. *J. Phys. Chem. Lett.* **2015**, *6*, 586.

(29) The pyrene ligand is trapped in its oxidized form until a subsequent redox couple, that can mediate its discharge, is reached. Under these conditions, one would expect a catalytic wave at the onset of the $TTF^{(\bullet+)}$ reduction and positive of the formal potential of the $TTF^{(\bullet+)}$/TTF couple.

DOI: 10.1021/jacs.6b09880
J. Am. Chem. Soc. 2016, 138, 14242−14245